Journal of Computational Physics 497 (2024) 112619

Contents lists available at ScienceDirect

Journal of Computational Physics

journal homepage: www.elsevier.com/locate/jcp

Adjoint-based estimation of sensitivity of clinical measures to boundary conditions for arteries ☆

Rainald Löhner [a,*], Harbir Antil [b], Fernando Mut [c], Juan Cebral [c]

[a] Center for Computational Fluid Dynamics, George Mason University, 4400 University Dr., Fairfax, 22030-4444, VA, USA
[b] Center for Mathematics and Artificial Intelligence, George Mason University, 4400 University Dr., Fairfax, 22030-4444, VA, USA
[c] Dept. of Biomedical Engineering, George Mason University, 4400 University Dr., Fairfax, 22030-4444, VA, USA

ARTICLE INFO

This paper is dedicated to Prof. Roland Glowinski

Keywords:
Incomplete boundary conditions
Adjoint solvers
CFD
Sensitivity analysis

ABSTRACT

The use of adjoint solvers is considered in order to obtain the sensitivity of clinical measures in aneurysms to incomplete (or unknown) boundary conditions and/or geometry. It is shown that these techniques offer interesting theoretical insights and viable computational tools to obtain these sensitivities. A optimization framework with Navier-Stokes equations (in the laminar regime) as constraints is introduced. Sensitivities with respect to inflow and inflow position are derived. In the specific case of inflow normal to the boundary, the sensitivities are shown to be the function of adjoint pressure. For the Poiseuille flow through a channel, explicit expressions for all the underlying quantities such as solution to the state equations, adjoint equations and sensitivites are derived, which are further confirmed by numerical experiments. In the next two examples, flow inside aneurysm geometries is considered.

1. Introduction

The analysis of haemodynamic phenomena and their clinical relevance via computational mechanics (fluids, solids, …) is now common in research and development. Yet a recurring question has been the influence of boundary conditions and geometry on 'clinically relevant measures'. As an example, consider flows in aneurysms, which are thought to be one of the primary drivers of aneurysm wall degeneration leading to destabilization, growth and eventual rupture [45,36]. Because the risk of aneurysm rupture is small (less than 1% annually [36]) but devastating, and the risk of complications during interventions is still significant (approximately 10% combined [23,27]), it is very important to identify high risk aneurysms for immediate treatment and low risk aneurysms for conservative observation and management. In addition, aneurysm treatment with devices that deviate the flow away from the aneurysm and promote aneurysm occlusion via intra-saccular thrombosis (so called flow diverting devices), has become a common strategy for complex aneurysms that are difficult to treat with open surgery or endovascular coils [27]. However, with this approach, many aneurysms remain open for a long time after treatment (e.g. over 9 months), and thus are still exposed to rupture risks. For these reasons, many investigations have focused on understanding the links between flow conditions and clinical outcomes, including aneurysm growth and rupture as well as occlusion and healing after treatment with flow diverters. Several studies have

☆ HA is partially supported by National Science Foundation (NSF) grants DMS-2110263, DMS-1913004 and the Air Force Office of Scientific Research under Award NO: FA9550-22-1-0248.

* Corresponding author.
E-mail addresses: rlohner@gmu.edu (R. Löhner), hantil@gmu.edu (H. Antil), fmut@gmu.edu (F. Mut), jcebral@gmu.edu (J. Cebral).
URLs: http://www.science.cfd.gmu.edu (R. Löhner), http://www.cmai.gmu.edu (H. Antil), http://www.gmu.edu (F. Mut), http://www.gmu.edu (J. Cebral).

https://doi.org/10.1016/j.jcp.2023.112619
Received 11 January 2023; Received in revised form 5 October 2023; Accepted 29 October 2023

Available online 7 November 2023

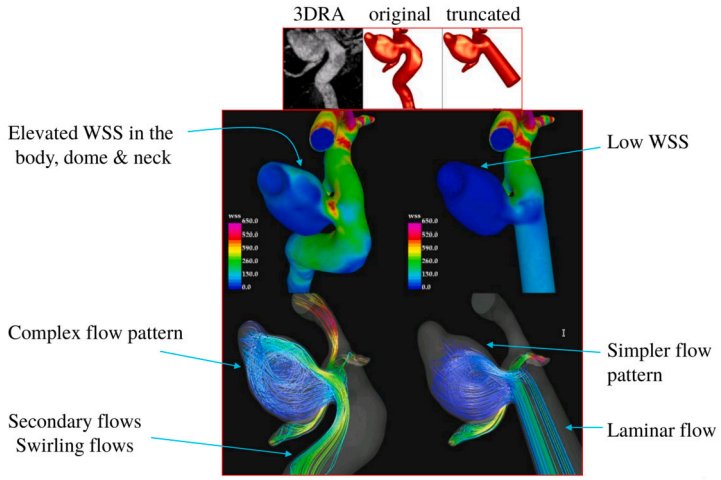

Fig. 1. Vessel 1: Difference in flow features between properly resolved and unresolved upstream geometry.

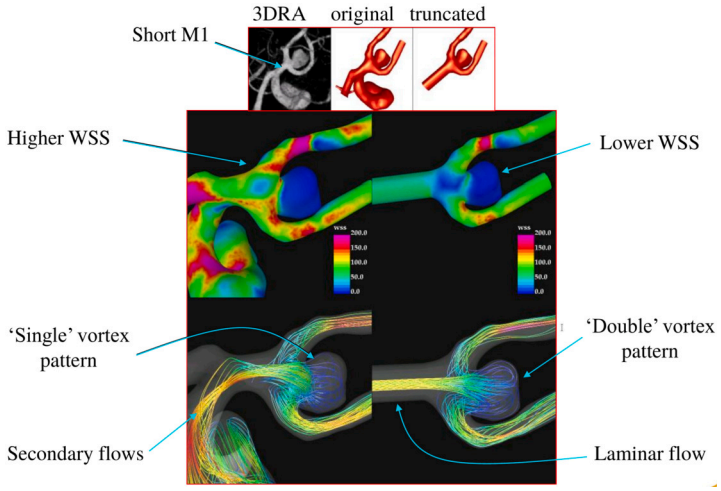

Fig. 2. Vessel 2: Difference in flow features between properly resolved and unresolved upstream geometry.

proposed to use different CFD-derived hemodynamic parameters to characterize the aneurysm hemodynamic environment and discriminate between ruptured and unruptured aneurysms [28,38,37,41,32,6,8]. Recently, hemodynamic variables have been combined with geometric, anatomical, and clinical parameters into statistical and machine learning models to identify aneurysms at risk of rupture [9,22,15,40,1] and/or destabilization and growth [42,39]. In parallel, the changes in hemodynamic conditions caused by the implantation of flow diverting devices have been investigated as possible predictors of outcomes of these endovascular treatments [21,24,42,30]. However, several of these studies suffer from an important limitation: to simplify and accelerate the vascular modeling, mesh generation, and flow simulation, arterial branches, including the inflow vessel are truncated, sometimes too close to the aneurysm. A crucial question is how far upstream the geometry has to be modeled accurately in order to obtain sufficiently accurate flow predictions, as well as their associated loads on vessel walls (shear, pressures) and clinically relevant measures (such as kinetic and vortical energy, vortex line length, etc.). In many cases, users may not have sufficient upstream information, so this question is of high relevance. The thesis of Castro and subsequent publications [4,5] have shown how dramatic the difference between well resolved upstream geometries and so-called 'cut' geometries can be. In some cases, completely different types of flow were seen, which in turn could have led to different clinical decisions. Figs. 1-2 show two examples.

To complicate matters further, the flow is transient/pulsating, and the flowrate and flow profile coming in at the upstream boundary in most cases is unknown. It is a common practice to simply set some kind of pipe flow profile (Poiseuille, Womersley) at the inflow, adjusting the analytical parameters to the estimated/known flux.

The central question remains: *what is the influence of a change of boundary conditions (e.g. inflow profiles) or geometry (e.g. more upstream/downstream geometry) on the clinically relevant measures ?*

A simple way to answer this question is to perform several runs, each with a different geometry or different boundary condition. This finite difference approach can then yield the sensitivity of a 'measure of clinical relevance' I to a change in geometry or boundary condition z. Another possibility is via adjoints [25,43,18,17,3]. We also refer to a series of works by Glowinski and collaborators

on the role of adjoints in optimization [12,16,34,2,11,13]. See also [35,19,14]. We emphasize that this list is incomplete as many authors have made fundamental contributions to this topic.

1.1. Upstream boundary conditions for the flow

It is known from empirical evidence and simple fluid mechanics that given any steady inflow velocity profile, after a given number of diameters along the pipe the flow will revert to a simple pipe flow (Poiseuille). This so-called hydrodynamic entry length L_h is a function of the Reynolds number Re, and for laminar flow and uniform inflow is given by:

$$L_h = 0.05 Re\ d\,, \quad Re = \frac{\rho U_e\ d}{\mu}\,, \tag{1}$$

where ρ, U_e, μ denote the density, mean entrance velocity and viscosity of the flow and d the vessel diameter. For blood and a typical artery $\rho = 1\ g/cm^3, U_e = 50\ cm/sec, \mu = 0.04\ g/cm/sec,\ d = 0.1\ cm$, so $Re = O(100)$ and $L_h = 5\ d$. Note that this estimate is only valid for steady flows and a uniform inflow. As far as the authors are aware, similar estimates for vessels with high curvatures (tortuosity) as typically encountered in arteries are not available. We note in passing that for the unsteady cases analyzed by [4,5] the number of upstream diameters required before the flow did not change in the aneurysms was much higher than the estimate given above.

1.2. Possible mathematical approaches

In order to formulate the problem mathematically, we can consider different approaches.

a) Empirical Data: for any given geometry/case, one could perform a series of studies, changing the type of inflow (vortical flows, unsteady flows) and seeing how long the observed hydrodynamic entry lengths are;
b) Sensitivity Analysis I: one could try to obtain a 'topological derivative' that measures the sensitivity of the flow in the aneurysm with respect to movement of the upstream boundary.
c) Sensitivity Analysis II: one could obtain a 'flow derivative' that measures the sensitivity of the clinical measure of the flow in the aneurysm with respect to changes of the entry flow in the upstream boundary.

Outline: The remainder of the paper is organized as follows. In Section 2, we first introduce a generic optimization problem formulation and adjoint framework. This generic discussion is well-known. This is followed by an example of Navier-Stokes specific to the aneurysm problem. We study the sensitivity with respect to the inflow velocity and inflow position. Section 3 focuses on numerical implementation. In Section 4.1, we present a specific example corresponding to the 2-D channel flow. For this example, we are able to derive explicit expressions for the state variables, adjoint variables, and the sensitivities (see Appendix A). This is followed by a realistic aneurysm example in Section 4.3, where we study the sensitivity of the 'measure of clinical relevance' I. All the numerical examples confirm the proposed approach.

2. General adjoint formulation

Suppose we have a 'measure of clinical relevance' I for a region that is in or close to an aneurysm. This could be the kinetic or vortical energy, the shear stress or the length of vortex lines - all of which have been proposed in the literature [31,7,10].

The question then becomes: how sensitive is this measure to the (often unknown) boundary conditions imposed or the (often approximate) geometric accuracy? Given that I is a function of the unknowns u and these in turn are a function of a set of parameters z describing the boundary conditions or the geometry, the answer to this question is given by the gradient of I. Consider the well-known generic minimization problem

$$\min_{u,z} I(u,z) \quad \text{subject to} \quad e(u,z) = 0\,,$$

where $I : U \times Z \to \mathbb{R}$ is the cost functional and $e(\cdot,\cdot) : U \times Z \to Y$ is the PDE constraint. Here U, Y and Z are function spaces. Typically, U, Y are Banach spaces and Z is a Hilbert space. Under very generic conditions, one can establish existence of solution to the above optimization problems, see [17,3]. As it has been known in the literature, there are two ways to derive the expression of the adjoint and the gradient of objective function I. The first approach is the so-called reduced formulation, where assuming that the PDE is uniquely solvable, one considers the well-defined control-to-state map

$$z \mapsto u(z)$$

with $(u(z), z)$ solving the PDE $e(u(z), z) = 0$. The reduced objective functional is then given by $\mathcal{I}(z) = I(u(z), z)$. Then one obtains the derivative of $\mathcal{I}$ with respect to z which also requires computing the sensitivites of u with respect to z. The second approach is the full space formulation and it requires forming the Lagrangian. Under fairly generic conditions (constraint qualifications), one can establish the existence of Lagrange multipliers in this setting, see [46,17]. Regardless, in both cases, the same expression of gradient is obtained [3, Pg. 14].

We briefly sketch the Lagrangian approach and refer to [17,3] for details. Let p denotes the adjoint variable, then the Lagrangian functional is given by

$$L(u,z,p) = I(u,z) - \langle e(u,z), p\rangle_{Y,Y^*}. \tag{2}$$

Then at a stationary point (u,z,p) the following conditions hold

$$\begin{aligned} L_p(u,z,p) &= 0, \\ L_u(u,z,p) &= 0, \\ L_z(u,z,p) &= 0. \end{aligned} \tag{3}$$

Our goal for the application under consideration is not to solve the above optimization problem, but rather derive the expression of the gradient $L_z(u,z,p)$. In view of the expression of the Lagrangian given in (2), it is not difficult to see that conditions in (3) are equivalent to

$$\begin{aligned} e(u,z) &= 0, && \text{(State equation)} \\ e_u(u,z)^* p &= I_u(u,z), && \text{(Adjoint equation)} \\ I_z(u,z) - e_z(u,z)^* p &= 0. && \text{(Gradient equation)} \end{aligned} \tag{4}$$

Namely, the gradient is given by (cf. [3, Pg. 14])

$$\nabla \mathcal{I}(z) = I_z(u,z) - e_z(u,z)^* p. \tag{5}$$

The consequences of the above formulation are profound:

- The variation of I in (5) exhibits only derivatives with respect to z, i.e., no explicit derivatives with respect to u appear;
- The cost of evaluation of gradients is independent of the number of design variables (!).

In the next section, we will apply this abstract framework to the case where the PDE $e(u,z) = 0$ is given by the incompressible Navier-Stokes equations. These equations are used to model the flow in the aneurysms.

2.1. Incompressible Navier-Stokes and sensitivity with respect to inflow

Let the domain $\Omega \subset \mathbb{R}^d$ be sufficiently smooth, and consisting of two subdomains Ω_{aneurysm} and the remainder of the domain $\Omega \setminus \Omega_{\text{aneurysm}}$ consisting of vascular vessels. Furthermore, let the boundary Γ of Ω consist of three parts Γ_{in} (inflow), Γ_{fixed} (fixed / wall), and Γ_{out} (outflow). Moreover, let $(\boldsymbol{u}, p)$ denote the velocity-pressure pair solving the incompressible Navier-Stokes equations:

$$\begin{aligned} -\text{div}(\mu \nabla \boldsymbol{u}) + (\boldsymbol{u}\cdot\nabla)\boldsymbol{u} + \nabla p &= \boldsymbol{f} && \text{in } \Omega \\ \text{div } \boldsymbol{u} &= 0 && \text{in } \Omega \\ \boldsymbol{u} &= \boldsymbol{z} && \text{on } \Gamma_{\text{in}} \\ \boldsymbol{u} &= \boldsymbol{0} && \text{on } \Gamma_{\text{fixed}} \\ (\mu \nabla \boldsymbol{u} - p\boldsymbol{I})\cdot \boldsymbol{n} &= \boldsymbol{0} && \text{on } \Gamma_{\text{out}} \end{aligned} \tag{6}$$

where $\boldsymbol{f}$ denotes a given force (for the current set of applications $\boldsymbol{f} = 0$), μ is viscosity, $\boldsymbol{I}$ is the identity tensor, and $\boldsymbol{n}$ is the outward unit normal. Finally, $\boldsymbol{z}$ is some given velocity profile on the inflow boundary Γ_{in}.

Given a quantity of interest (measure of clinical relevance), $I(\boldsymbol{u}, p, \boldsymbol{z})$, the goal is to obtain the derivative of I with respect $\boldsymbol{z}$ with the help of adjoint formulation as discussed in the previous section. We begin by stating the following result, see [44, Appendix C]

Lemma 1. *Let $\boldsymbol{u}$, $\boldsymbol{v}$ and $\tilde{\boldsymbol{u}}$ be smooth vector fields, then*

$$\int_\Omega [(\boldsymbol{u}\cdot\nabla)\boldsymbol{v}]\tilde{\boldsymbol{u}}\ \text{dx} = -\int_\Omega (div\ \boldsymbol{u})(\boldsymbol{v}\cdot\tilde{\boldsymbol{u}}) + [(\boldsymbol{u}\cdot\nabla)\tilde{\boldsymbol{u}}]\cdot\boldsymbol{v}\ \text{dx} + \int_\Gamma (\boldsymbol{u}\cdot\boldsymbol{n})(\boldsymbol{v}\cdot\tilde{\boldsymbol{u}})\ \text{ds}.$$

When $\boldsymbol{v} = \boldsymbol{u}$ and div $\boldsymbol{u} = 0$, then

$$\int_\Omega [(\boldsymbol{u}\cdot\nabla)\boldsymbol{u}]\tilde{\boldsymbol{u}}\ \text{dx} = -\int_\Omega [(\boldsymbol{u}\cdot\nabla)\tilde{\boldsymbol{u}}]\cdot\boldsymbol{u}\ \text{dx} + \int_\Gamma (\boldsymbol{u}\cdot\boldsymbol{n})(\boldsymbol{u}\cdot\tilde{\boldsymbol{u}})\ \text{ds}.$$

Next, a derivation of sensitivity is provided using the adjoint approach. We denote the partial derivative of I with respect to $\boldsymbol{u}$, $\boldsymbol{z}$ and p, respectively by $I_{\boldsymbol{u}}$, $I_{\boldsymbol{z}}$ and I_p. We begin by writing the Lagrangian functional

$$L(\boldsymbol{u},p,\tilde{\boldsymbol{u}},\tilde{p},\tilde{\boldsymbol{u}}_\Gamma) = I(\boldsymbol{u},p,\boldsymbol{z}) - \Bigg[\int_\Omega \left(-\mathrm{div}(\mu\nabla\boldsymbol{u}) + (\boldsymbol{u}\cdot\nabla)\boldsymbol{u} + \nabla p - \boldsymbol{f}\right)\cdot\tilde{\boldsymbol{u}} - \tilde{p}\,\mathrm{div}\,\boldsymbol{u}\,\mathrm{dx} + \int_{\Gamma_{\text{in}}} (\boldsymbol{u}-\boldsymbol{z})\cdot\tilde{\boldsymbol{u}}_\Gamma\,\mathrm{ds}\Bigg].$$

Applying integration-by-parts, and using Lemma 1, along with $\boldsymbol{u}=0$ on Γ_{fixed} and $(\mu\nabla\boldsymbol{u} - p\boldsymbol{1})\boldsymbol{n}=0$ on Γ_{out}, we obtain that

$$L(\boldsymbol{u},p,\tilde{\boldsymbol{u}},\tilde{p},\tilde{\boldsymbol{u}}_\Gamma) = I(\boldsymbol{u},p,\boldsymbol{z}) - \Bigg[\int_\Omega \mu\nabla\boldsymbol{u} : \nabla\tilde{\boldsymbol{u}} - [(\boldsymbol{u}\cdot\nabla)\tilde{\boldsymbol{u}}]\cdot\boldsymbol{u} - p\,\mathrm{div}\,\tilde{\boldsymbol{u}} + \boldsymbol{u}\cdot\nabla\tilde{p}\,\mathrm{dx} + \int_{\Gamma_{\text{in}}\cup\Gamma_{\text{fixed}}} \tilde{\boldsymbol{u}}\cdot(-\mu\nabla\boldsymbol{u} + p\boldsymbol{I})\,\boldsymbol{n}\,\mathrm{ds} - \int_{\Gamma_{\text{in}}\cup\Gamma_{\text{out}}} \boldsymbol{u}\cdot\boldsymbol{n}\tilde{p}\,\mathrm{ds} + \int_{\Gamma_{\text{in}}} (\boldsymbol{u}-\boldsymbol{z})\cdot\tilde{\boldsymbol{u}}_\Gamma\,\mathrm{ds} + \int_{\Gamma_{\text{in}}\cup\Gamma_{\text{out}}} (\boldsymbol{u}\cdot\boldsymbol{n})(\boldsymbol{u}\cdot\tilde{\boldsymbol{u}})\mathrm{ds}\Bigg].$$

Applying integration-by-parts again, we arrive at

$$\begin{aligned} L(\boldsymbol{u},p,\tilde{\boldsymbol{u}},\tilde{p},\tilde{\boldsymbol{u}}_\Gamma) = I(\boldsymbol{u},p,\boldsymbol{z}) - \Bigg[&\int_\Omega \left(-\mathrm{div}(\mu\nabla\tilde{\boldsymbol{u}}) + \nabla\tilde{p}\right)\cdot\boldsymbol{u} - [(\boldsymbol{u}\cdot\nabla)\tilde{\boldsymbol{u}}]\cdot\boldsymbol{u} - p\,\mathrm{div}\,\tilde{\boldsymbol{u}}\,\mathrm{dx} \\ &+ \int_{\Gamma_{\text{in}}\cup\Gamma_{\text{fixed}}} \tilde{\boldsymbol{u}}\cdot(-\mu\nabla\boldsymbol{u} + p\boldsymbol{I})\,\boldsymbol{n}\,\mathrm{ds} + \int_{\Gamma_{\text{in}}} \boldsymbol{u}\cdot(\mu\nabla\tilde{\boldsymbol{u}} - \tilde{p}\boldsymbol{I})\boldsymbol{n}\,\mathrm{ds} \\ &+ \int_{\Gamma_{\text{out}}} \boldsymbol{u}\cdot(\mu\nabla\tilde{\boldsymbol{u}} - \tilde{p}\boldsymbol{I})\boldsymbol{n}\,\mathrm{ds} \\ &+ \int_{\Gamma_{\text{in}}} (\boldsymbol{u}-\boldsymbol{z})\cdot\tilde{\boldsymbol{u}}_\Gamma\,\mathrm{ds} + \int_{\Gamma_{\text{in}}\cup\Gamma_{\text{out}}} (\boldsymbol{u}\cdot\boldsymbol{n})(\boldsymbol{u}\cdot\tilde{\boldsymbol{u}})\mathrm{ds}\Bigg]. \end{aligned} \tag{7}$$

In view of (3), taking a variation of L with respect to $(\boldsymbol{u},p)$ and setting it equal to zero, we obtain the adjoint equation

$$\begin{aligned} -\mathrm{div}(\mu\nabla\tilde{\boldsymbol{u}}) - (\boldsymbol{u}\cdot\nabla)\tilde{\boldsymbol{u}} - (\nabla\tilde{\boldsymbol{u}})^\top\boldsymbol{u} + \nabla\tilde{p} &= I_{\boldsymbol{u}}(\boldsymbol{u},p,\boldsymbol{z}) \quad \text{in } \Omega \\ \mathrm{div}\,\tilde{\boldsymbol{u}} &= -I_p(\boldsymbol{u},p,\boldsymbol{z}) \quad \text{in } \Omega \\ \tilde{\boldsymbol{u}} &= \boldsymbol{0} \quad \text{on } \Gamma_{\text{in}}\cup\Gamma_{\text{fixed}} \\ (\mu\nabla\tilde{\boldsymbol{u}} - \tilde{p}\boldsymbol{I})\boldsymbol{n} &= -[(\boldsymbol{u}\cdot\tilde{\boldsymbol{u}})\boldsymbol{n} + (\boldsymbol{u}\cdot\boldsymbol{n})\tilde{\boldsymbol{u}}] \quad \text{on } \Gamma_{\text{out}}. \end{aligned} \tag{8}$$

We note the compatibility condition:

$$\tilde{\boldsymbol{u}}_\Gamma = -(\mu\nabla\tilde{\boldsymbol{u}} - \tilde{p}\boldsymbol{I})\boldsymbol{n} - (\boldsymbol{u}\cdot\tilde{\boldsymbol{u}})\boldsymbol{n} - (\boldsymbol{u}\cdot\boldsymbol{n})\tilde{\boldsymbol{u}} = -(\mu\nabla\tilde{\boldsymbol{u}} - \tilde{p}\boldsymbol{I})\boldsymbol{n} \quad \text{on } \Gamma_{\text{in}},$$

where in the last equality we used the fact that $\tilde{\boldsymbol{u}}=\boldsymbol{0}$ on Γ_{in}. We notice that, if I is independent of p, then we obtain the standard incompressibility condition for $\tilde{\boldsymbol{u}}$ in (8). Finally, the required variation of I with respect to $\boldsymbol{z}$ is given by

$$\begin{aligned} D_{\boldsymbol{z}} I(\boldsymbol{u},p,\boldsymbol{z}) &= I_{\boldsymbol{z}}(\boldsymbol{u},p,\boldsymbol{z}) - [(\mu\nabla\tilde{\boldsymbol{u}} - \tilde{p}\boldsymbol{I})\boldsymbol{n} + (\boldsymbol{u}\cdot\tilde{\boldsymbol{u}})\boldsymbol{n} + (\boldsymbol{u}\cdot\boldsymbol{n})\tilde{\boldsymbol{u}}] \quad \text{on } \Gamma_{\text{in}} \\ &= I_{\boldsymbol{z}}(\boldsymbol{u},p,\boldsymbol{z}) - [(\mu\nabla\tilde{\boldsymbol{u}} - \tilde{p}\boldsymbol{I})\boldsymbol{n}] \quad \text{on } \Gamma_{\text{in}}, \end{aligned} \tag{9}$$

where we have again used the fact that $\tilde{\boldsymbol{u}}=\boldsymbol{0}$ on Γ_{in}. Note that if the clinical measure I is not a function of the control variable (in this case the inflow velocity), for a channel with constant flow in the normal direction $\boldsymbol{n}$ (i.e. $\mu\nabla\tilde{\boldsymbol{u}}\cdot\boldsymbol{n}=0$) the sensitivity reverts to (recall that $\mathcal{I}$ is the reduced objective)

$$D_{\boldsymbol{z}}\mathcal{I}(\boldsymbol{z}) = \tilde{p}\boldsymbol{n} \quad \text{on } \Gamma_{\text{in}}. \tag{10}$$

i.e. *the sensitivity to inflow velocities is the adjoint pressure*.

2.1.1. Sensitivity to changes in inflow position

Consider next the variation of the Lagrangian L given in (7) with respect to the normal $\boldsymbol{n}$. We recall that after simplifications, we have

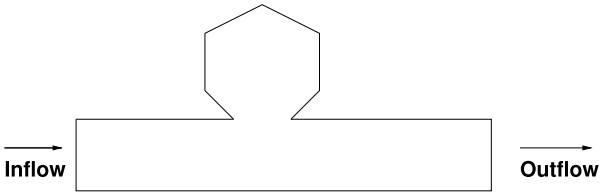

Fig. 3. Schematic of Aneurysm.

$$L(\boldsymbol{u},p,\tilde{\boldsymbol{u}},\tilde{p},\tilde{\boldsymbol{u}}_\Gamma) = I(\boldsymbol{u},p,\boldsymbol{z}) - \int_{\Gamma_{\text{in}}} (\boldsymbol{u}-\boldsymbol{z})\,[(\mu\nabla\tilde{\boldsymbol{u}} - \tilde{p}\boldsymbol{I})\boldsymbol{n}]\ \text{ds}\,.$$

Then

$$\begin{aligned} D_{\boldsymbol{n}} L(\boldsymbol{u},p,\tilde{\boldsymbol{u}},\tilde{p},\tilde{\boldsymbol{u}}_\Gamma)\boldsymbol{h} &= D_{\boldsymbol{n}} I(\boldsymbol{u},p,\boldsymbol{z})\boldsymbol{h} - \int_{\Gamma_{\text{in}}} D_{\boldsymbol{n}}\,[(\boldsymbol{u}-\boldsymbol{z})((\mu\nabla\tilde{\boldsymbol{u}} - \tilde{p}\boldsymbol{I})\boldsymbol{n})]\,\boldsymbol{h}\ \text{ds} \\ &= D_{\boldsymbol{n}} I(\boldsymbol{u},p,\boldsymbol{z})\boldsymbol{h} - \int_{\Gamma_{\text{in}}} (D_{\boldsymbol{n}}\boldsymbol{u}\boldsymbol{h})\,[((\mu\nabla\tilde{\boldsymbol{u}} - \tilde{p}\boldsymbol{I})\boldsymbol{n})] + (\boldsymbol{u}-\boldsymbol{z})D_{\boldsymbol{n}}\,[((\mu\nabla\tilde{\boldsymbol{u}} - \tilde{p}\boldsymbol{I})\boldsymbol{n})]\,\boldsymbol{h}\ \text{ds} \\ &= D_{\boldsymbol{n}} I(\boldsymbol{u},p,\boldsymbol{z})\boldsymbol{h} - \int_{\Gamma_{\text{in}}} (D_{\boldsymbol{n}}\boldsymbol{u}\boldsymbol{h})\,[((\mu\nabla\tilde{\boldsymbol{u}} - \tilde{p}\boldsymbol{I})\boldsymbol{n})]\ \text{ds}\,, \end{aligned}$$

where, in the last step, we have used the fact that $\boldsymbol{u}=\boldsymbol{z}$ on Γ_{in}. In case, I is independent of $\boldsymbol{n}$, we then obtain that

$$D_{\boldsymbol{n}} L(\boldsymbol{u},p,\tilde{\boldsymbol{u}},\tilde{p},\tilde{\boldsymbol{u}}_\Gamma)\boldsymbol{h} = -\int_{\Gamma_{\text{in}}} (D_{\boldsymbol{n}}\boldsymbol{u}\boldsymbol{h})\,[((\mu\nabla\tilde{\boldsymbol{u}} - \tilde{p}\boldsymbol{I})\boldsymbol{n})]\ \text{ds}\,.$$

Note that if $\mu\nabla\tilde{\boldsymbol{u}}\cdot\boldsymbol{n}=0$ (as is often the case) the sensitivity reverts to (recall that $\mathcal{I}$ is the reduced objective)

$$D_{\boldsymbol{n}}\mathcal{I}(\boldsymbol{n}) = u_n^n\tilde{p} \quad \text{on } \Gamma_{\text{in}} \tag{11}$$

i.e. *the sensitivity to changes in inflow position is the adjoint pressure multiplied by the normal derivative of the inflow velocity*.

2.2. In- and outflow boundary conditions for the adjoint

Consider the aneurysm shown in Fig. 3.

For the usual (forward) incompressible Navier-Stokes calculation, one would prescribe a velocity profile ($\boldsymbol{u}=\boldsymbol{z}$) at the inflow boundary and the 'do nothing' ($(\eta\nabla\boldsymbol{u} - p\boldsymbol{I})\boldsymbol{n}=0$) or pressure boundary condition ($p = p_{\text{ out}}$) at the outflow boundary. This implies letting the pressure 'free' at the inflow and the velocity 'free' at the outflow. At the walls the velocity is zero, i.e. $\boldsymbol{u}|_{\Gamma_{\text{fixed}}} = \boldsymbol{0}$. Consider now the adjoint problem. The boundary conditions in this case are described in (8), i.e., we obtain zero velocity at the inflow and 'do nothing' or prescribed zero adjoint pressure at the outflow. The adjoint velocity is also zero on the walls.

3. Numerical implementation

In a strict mathematical sense, the adjoint solver obtained by discretizing the adjoint partial differential equation should be as close as possible to the discrete adjoint obtained from transposing and manipulating the discretization of the forward problem. In this way 'optimize-then-discretize' and 'discretize-then-optimize' are as close as possible. This was not adopted in the present case. Instead, while the forward problem was solved for the incompressible Navier-Stokes equations, the adjoint equations were derived for the quasi-incompressible Navier-Stokes equations, which for steady flows give the same results. The forward problem was integrated to steady state using a fractional step solver with implicit solution of the viscous terms and the pressure increments using an edge-based formulation of linear finite elements (tetrahedra). The adjoint was discretized using edge-based upwinding for the velocities and 4th order pressure stabilization [26]. For each point i in the mesh this scheme is given by:

$$\left[\mathbf{A}^k\right]_i^T M_i\nabla^k(\tilde{\boldsymbol{u}})_i + (\mu_i+\mu_j)K_{ij}(\tilde{\boldsymbol{u}}_i - \tilde{\boldsymbol{u}}_j) + M_i I_{\boldsymbol{u}}^{\Omega} + D_i = 0\,, \tag{12}$$

where $\mathbf{A}, M_i, \nabla^k, K_{ij}, D_i$ denote the Jacobians of the advective fluxes, lumped mass-matrix, discrete gradient in direction k, Laplacian edge-based coefficients and damping vector, and

$$\nabla^k(\tilde{\boldsymbol{u}})_i = C_{ij}^k(\tilde{\boldsymbol{u}}_i + \tilde{\boldsymbol{u}}_j)\,,$$

where C_{ij}^k are the edge-based coefficients for the gradient (see [26], Chapter 20). Furthermore

$$D_i = -\lambda^{(ij)}\left[\tilde{\boldsymbol{u}}_i - \tilde{\boldsymbol{u}}_j + \frac{\beta}{2}\mathbf{l}_{ij}\cdot(\nabla(\tilde{\boldsymbol{u}})_i + \nabla(\tilde{\boldsymbol{u}})_j)\right],$$

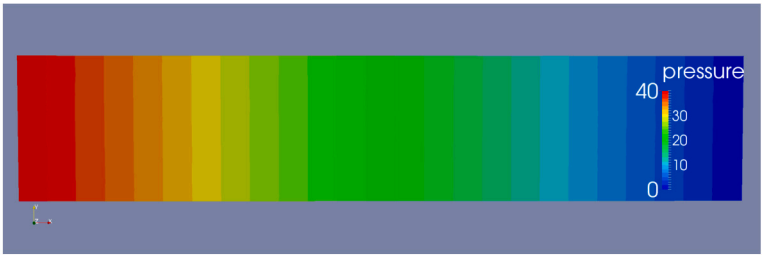

Fig. 4. Poiseuille Flow: Pressure.

where c is the speed of sound, $\tilde{p}$ the adjoint pressure, $\lambda = |\boldsymbol{u}| + c$ the maximum eigenvalue of the system, $\mathbf{l}_{ij} = \mathbf{x}_i - \mathbf{x}_j$ the edge-vector, i.e. the difference in the coordinates of nodes i, j and $0 < \beta < 1$ denotes a pressure sensor function of the form [33].

$$\beta = 1 - \frac{\tilde{p}_i - \tilde{p}_j + 0.5\mathbf{l}_{ij} \cdot (\nabla(\tilde{p})_i + \nabla(\tilde{p})_j)|}{|\tilde{p}_i - \tilde{p}_j| + |0.5\mathbf{l}_{ij} \cdot (\nabla(\tilde{p})_i + \nabla(\tilde{p})_j)|} \quad .$$

For $\beta = 0, 1$, second and fourth order damping operators are obtained respectively. Several other forms are possible for the sensor function β [29].

Although this discretization of the adjoint Euler fluxes looks like a blend of second and fourth order dissipation, it has no adjustable parameters. Defining $\boldsymbol{U} = (\boldsymbol{u}, p)$, $\tilde{\boldsymbol{U}} = (\tilde{\boldsymbol{u}}, \tilde{p})$ Eqn. (12) may be re-written as

$$\mathbf{R}(\boldsymbol{U}, \tilde{\boldsymbol{U}}) = 0\,,$$

the system re-written as an unsteady equation of the form:

$$\tilde{\boldsymbol{U}}_{,\tau} + \mathbf{R}(\boldsymbol{U}, \tilde{\boldsymbol{U}}) = 0\,,$$

and integrated in pseudo-time τ via a classic explicit multistep Runge-Kutta [20].

4. Numerical examples

We will focus on two main examples. At first, we consider Poiseuille flow through a channel in Section 4.1. Remarkably enough, we are able to derive the explicit expressions for all the quantities, such as solution to the state equation, adjoint equation and sensitivities, see Appendix A. These theoretical results are also confirmed by numerical results. In Section 4.3, we focus on a realistic aneurysm scenario, where we truly see the benefits of the proposed sensitivity approach.

4.1. Poiseuille flow

The 2-D channel flow provides a good test to verify the implementation of the forward and adjoint solvers. The domain considered is of dimension $0.0 \le x \le 0.5$, $-0.05 \le y \le 0.05$ and $-0.005 \le z \le 0.005$. A parabolic inflow with maximum velocity of $u_{max} = 1.0$ was prescribed. The velocity at the top and bottom walls (y_{min}, y_{max}) was prescribed to zero, and the velocity in the z-direction was prescribed to zero for the back and front walls (z_{min}, z_{max}). The other relevant parameter is $\mu = 0.01$. Two 'clinically relevant measures' (i.e. cost functions) were considered: kinetic energy $I = \frac{1}{2}\int_\Omega \rho \boldsymbol{u}^2 \, \mathrm{dx}$ and vortical energy $I = \frac{1}{2}\int_\Omega \rho |\nabla \times \boldsymbol{u}|^2 \, \mathrm{dx}$. We set $\rho = 1.0$ in our experiments. The derivation of the exact solutions for the adjoint equations for these cost functions may be found in Appendix A. Let $\boldsymbol{u} = (u, v, w)^\top$, then the x-component of $\boldsymbol{u}$ is given by:

$$u = \left[1 - \frac{4}{H^2} y^2\right] u_0\,,$$

where $u_0 = u_{max}$ and H is the total height of the channel, i.e. $y_{max} = -y_{min} = H/2$. We thus obtain

$$\partial_y u = -\frac{8u_0}{H^2} y, \quad \partial_{yy} u = -\frac{8u_0}{H^2}, \quad \partial_x p = -\frac{8\mu u_0}{H^2}.$$

The pressure, velocity magnitude, and velocity vectors are shown in Figs. 4-6.

4.1.1. Kinetic energy

Consider the cost function

$$I = \frac{1}{2}\int \rho |\boldsymbol{u}|^2 \, \mathrm{dx}\,,$$

implying

$$I_u = \rho u.$$

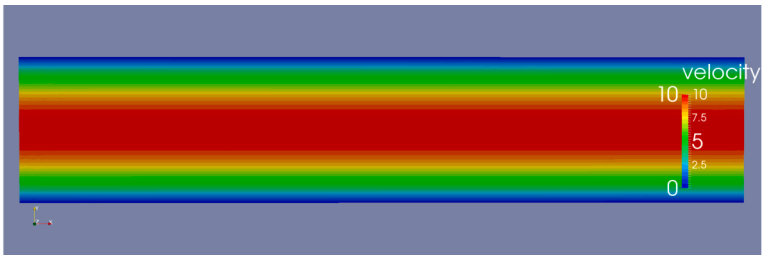

Fig. 5. Poiseuille Flow: Velocity Magnitude.

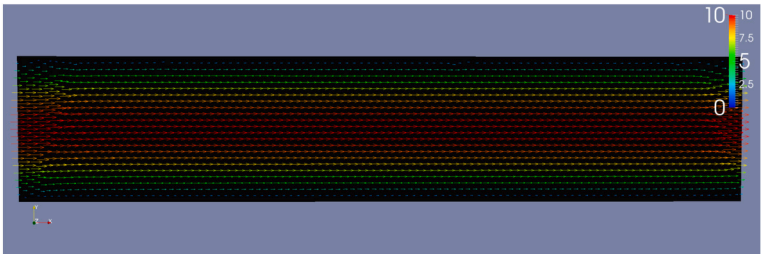

Fig. 6. Poiseuille Flow: Velocity.

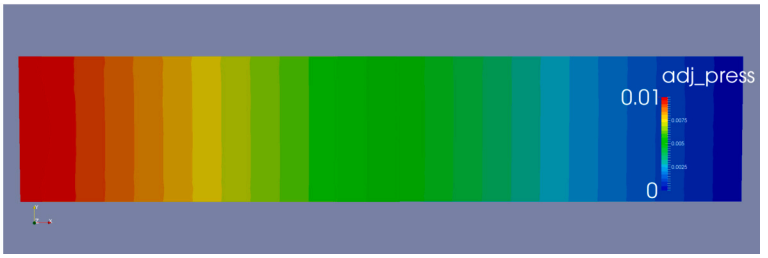

Fig. 7. Poiseuille Flow: Adjoint Pressure.

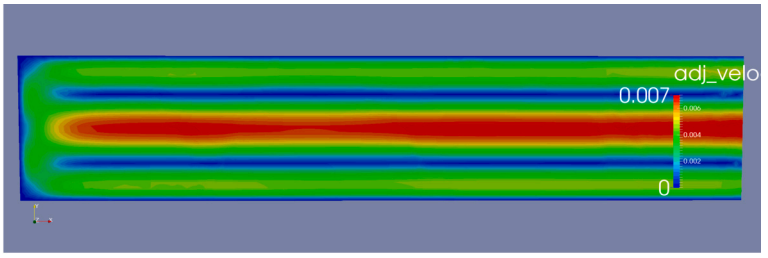

Fig. 8. Poiseuille Flow: Magnitude of Adjoint Velocity. Here the cost function is Kinetic Energy.

As can be seen in Appendix A, the adjoint pressure for this cost function is:

$$\partial_x \tilde{p} = \frac{4}{5}\rho u_0 \ ,$$

i.e. the gradient of the adjoint pressure is also constant and linearly dependent of u_0. The results obtained are shown in Figs. 7–9.

4.1.2. *Vortical energy*

The cost function is given by

$$I = \frac{1}{2}\int \rho\,|\nabla \times \boldsymbol{u}|^2 \ \mathrm{dx} \ .$$

For the 2-D channel $(u = u(y), v = 0, w = z)$

$$(\nabla \times \boldsymbol{u})^2 = \left(\partial_y u\right)^2 \ ,$$

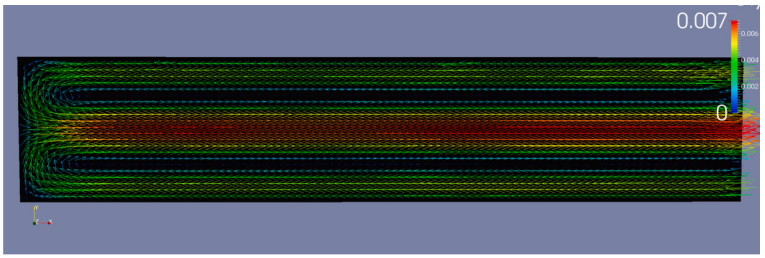

Fig. 9. Poiseuille Flow: Adjoint Velocity. Here the cost function is Kinetic Energy.

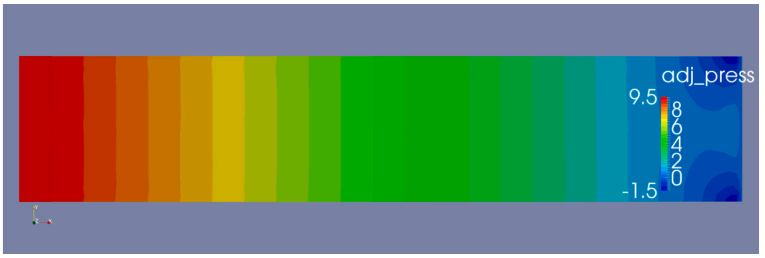

Fig. 10. Poiseuille Flow: Adjoint Pressure. Cost Function: Vortical Energy.

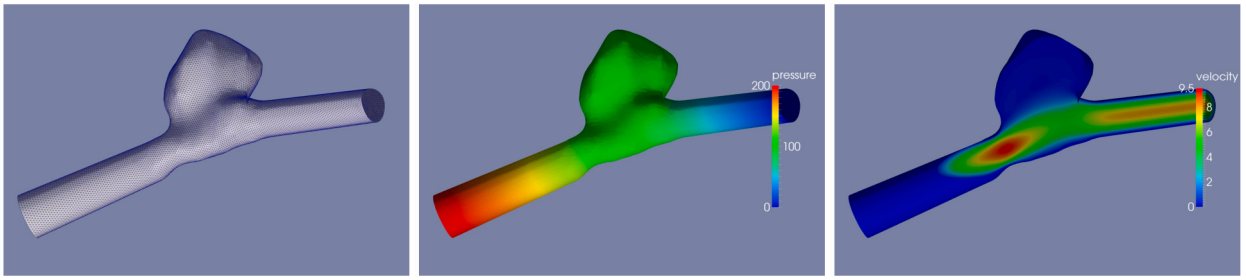

Fig. 11. a,b,c Aneurysm: Surface Triangulation, Surface Pressure and Magnitude of Velocity in Cut Plane.

so that

$$I_{,u} = \rho u_{,y}(u_{,y})_{,u} = -\rho u_{,yy} = -\frac{\rho}{\mu} p_{,x} \quad = \frac{8\rho u_0}{H^2} \quad ,$$

i.e. constant. As can be seen in Appendix A, the adjoint velocities and pressure are given by:

$$\tilde{u}(x,y) = 0 \quad , \quad \tilde{v}(x,y) = 0 \quad , -\tilde{p} = \frac{\rho}{\mu} p \quad .$$

(See Fig. 10.)

4.2. Aneurysm with simple flow pattern

As a more relevant example, we include an aneurysm with simple flow pattern. The geometry and discretization may be discerned from Figs. 11a-c which show the surface triangulation, pressure and magnitude of the velocity. The mesh consisted of about 470 K tetrahedra, 87 K points and 13.5 K boundary points. The region for the source-terms of the adjoint is shown in Fig. 12 a and the adjoint pressure, as well as the magnitude of the adjoint velocities obtained in Figs. 12 b,c. The adjoint velocites can also be seen in Figs. 13 a,b. Note the effect of the source-term that pushes the adjoint flow and forms a double vortex.

4.3. Aneurysm with complex flow pattern

As a second example, we include an aneurysm with a complex flow pattern. The geometry and discretization may be discerned from Figs. 14a-c which show the surface triangulation, pressure and magnitude of the velocity. The mesh consisted of 1.46M tetrahedra, 270 K points and 45 K boundary points. The region for the source-terms of the adjoint is shown in Fig. 15 a and the adjoint pressure, as well as the magnitude of the adjoint velocities obtained in Figs. 15 b,c. Note that at the inflow the adjoint pressure is not close to zero, indicating that the inflow section may have to be extended further in order to obtain reliable results.

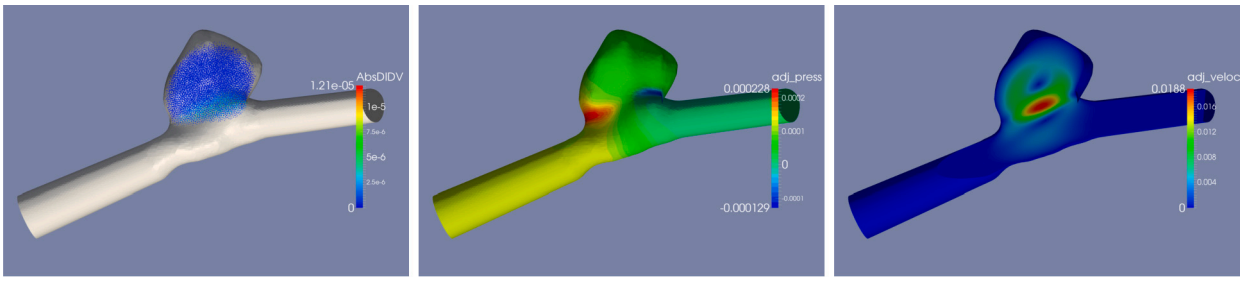

Fig. 12. a,b,c Aneurysm: Source, Adjoint Pressure and Magnitude of Adjoint Velocity in Cut Plane.

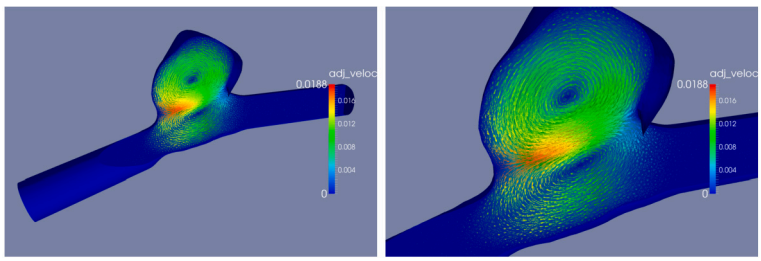

Fig. 13. a,b Aneurysm: Adjoint Velocity in Cut Plane.

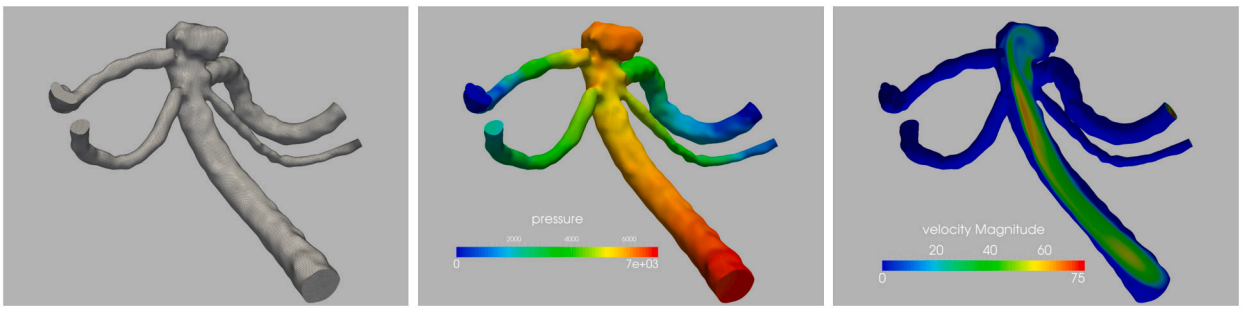

Fig. 14. a,b,c Aneurysm: Surface Triangulation, Surface Pressure and Magnitude of Velocity in Cut Plane.

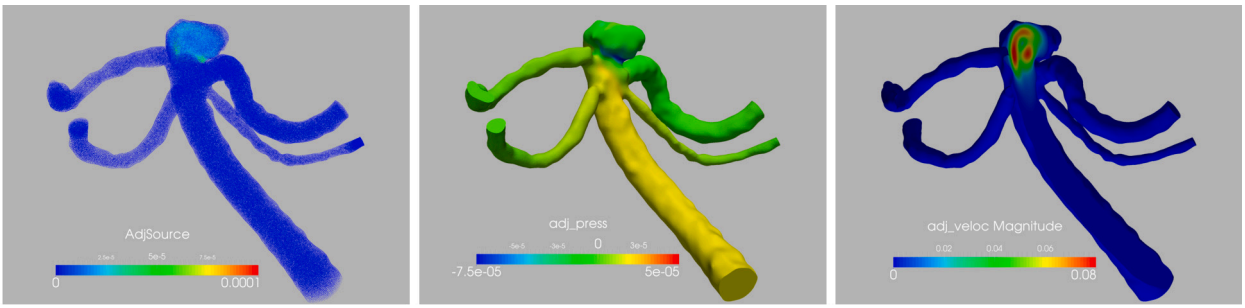

Fig. 15. a,b,c Aneurysm: Source, Adjoint Pressure and Magnitude of Adjoint Velocity in Cut Plane.

5. Conclusions and outlook

The use of adjoint solvers to assess the sensitivity of incomplete boundary (inflow, geometry) information has been considered. The results of this investigation indicate that the sensitivity of clinical measures or other flow features that are inside the flow domain with respect to inflow velocity is proportional to the adjoint pressure, while the sensitivity with respect to inflow geometry is given by the product of the adjoint pressure and the normal derivative of the inflow velocity. Thus, the adjoint pressure may be a good indicator to see if the inflow boundary of haemodynamic cases is far enough from the region of interest so that errors can be avoided. The use of adjoint solvers is not unproblematic. Unlike running a series of cases, varying inflow profiles and geometry, and seeing their influence on many clinically relevant measures, adjoints require a different run for each of the clinical measures.

Declaration of competing interest

The authors declare the following financial interests/personal relationships which may be considered as potential competing interests: Harbir Antil reports financial support was provided by National Science Foundation. Harbir Antil reports financial support was provided by AFOSR under Award NO: FA9550-22-1-0248.

Data availability

Data will be made available on request.

Appendix A. Analytical expressions for Poiseuille flow

A.1. Exact forward solution

Let us consider a long 2-D channel of length $0 \le x \le L$ and width $-H/2 \le y \le H/2$ with incompressible viscous flow. Let $\boldsymbol{u} = (u, v, w)^\top$, then the equation for the x-velocity u is given by:

$$u\partial_x u + v\partial_y u + \partial_x p = \mu \Delta u \,.$$

Assuming a constant velocity profile in x, i.e. $u = u(y)$ and laminar flow with $v = 0$, the solution is the Poiseuille solution, given by:

$$u = \left[1 - \frac{4}{H^2} y^2\right] u_0 \,, \tag{13}$$

where u_0 is the maximum velocity at the center of the channel, and the channel extends in height from $-H/2 \le y \le H/2$, implying

$$\partial_y u = -\frac{8u_0}{H^2} y \,,$$

and

$$\partial_{yy} u = -\frac{8u_0}{H^2} \,,$$

so that the constant pressure gradient is given by:

$$\partial_x p = -\frac{8\mu u_0}{H^2} \,,$$

where we have used the fact that $\partial_x u = \partial_{xx} u = 0$. The average velocity is then:

$$\overline{u} = \frac{1}{H} \int\limits_{-H/2}^{H/2} u \, \mathrm{d}y = \frac{2}{3} u_0 \,.$$

A.2. Adjoint equations

The equation for the adjoint x-velocity $\tilde{u}$ is given by:

$$-u\partial_x \tilde{u} - v\partial_y \tilde{u} + \partial_x \tilde{p} = \mu \Delta \tilde{u}_{,xx} + I_u$$

Here I is the cost function. For the channel u is given by (13) and $v = 0$.

Kinetic Energy: If the cost function is given by the kinetic energy

$$I = \frac{1}{2} \int \rho |\boldsymbol{u}|^2 \, \mathrm{d}x \,,$$

then

$$I_u = \rho u \,.$$

Assuming a long channel with no change in x of the variables, the equation for the adjoint x-velocity $\tilde{u}$ simplifies to:

$$\partial_x \tilde{p} = \mu \partial_{yy} \tilde{u} + \rho u_0 \left[1 - \frac{4}{H^2} y^2\right] .$$

Assuming furthermore that $\partial_x \tilde{p}$ is constant, and applying the boundary conditions $\tilde{u} = 0$ for $y = -H/2$ and $y = H/2$ this yields

$$\tilde{u} = \frac{1}{2\mu} \left[-\partial_x \tilde{p} + \rho u_0\right] \left[\frac{H^2}{4} - y^2\right] - \frac{\rho u_0}{3\mu H^2} \left[\frac{H^4}{16} - y^4\right] .$$

If we consider that at the inflow boundary $\tilde{u}=0$, then as the adjoint velocity field is also divergence-free, in any section of x we must have:

$$\int \tilde{u} dy = 0.$$

This implies:

$$\int_{-H/2}^{H/2} \tilde{u}\ \mathrm{dy} = \frac{1}{2\mu}\left[-\partial_x \tilde{p} + \rho u_0\right]\left[\frac{H^2}{4}y - \frac{y^3}{3}\right]_{-H/2}^{H/2} - \frac{\rho u_0}{3\mu H^2}\left[\frac{H^4}{16}y - \frac{y^5}{5}\right]_{-H/2}^{H/2} = 0.$$

Evaluation of all terms leads to the remarkable result:

$$\partial_x \tilde{p} = \frac{4}{5}\rho u_0 = -\frac{\rho H^2}{10\mu}\partial_x p,$$

i.e. the gradient of the adjoint pressure is also constant and linearly dependent of u_0. Given that the base level of the pressure p is arbitrary, we might set it so that it vanishes at the exit, i.e. $p=0$. We finally obtain the remarkable result that:

$$-\tilde{p} = \frac{\rho H^2}{10\mu} p,$$

i.e. the pressure and adjoint pressure are related by the factor $\frac{\rho H^2}{10\mu}$ and have a constant gradient in the field. The adjoint velocity is given by:

$$\tilde{u} = \frac{\rho u_0}{\mu}\left\{\frac{1}{10}\left[\frac{H^2}{4} - y^2\right] - \frac{1}{3H^2}\left[\frac{H^4}{16} - y^4\right]\right\}.$$

At the center of the channel the velocity is given by:

$$\tilde{u}(y=0) = \frac{\rho u_0 H^2}{240\mu}.$$

Vortical Energy: If the cost function is given by the vortical energy

$$I = \frac{1}{2}\int \rho\,|\nabla \times \boldsymbol{u}|^2\ \mathrm{dx},$$

then, for the 2-D channel ($u = u(y), v = 0, w = z$)

$$|\nabla \times \boldsymbol{u}|^2 = \left(\partial_y u\right)^2\ ,$$

so that

$$I_u = \rho \partial_y u (\partial_y u)_{,u} = -\rho \partial_{yy} u = -\frac{\rho}{\mu}\partial_x p = \frac{8\rho u_0}{H^2},$$

i.e. constant (!). Assuming a long channel with no change in x for the variables, the equation for the adjoint x-velocity $\tilde{u}$ simplifies to:

$$\partial_x \tilde{p} = \mu \partial_{yy}\tilde{u} - \frac{\rho}{\mu}\partial_x p.$$

As this is a long channel and the source-term is constant, the assumption that $\partial_x \tilde{p}$ is constant is warranted. This implies that $\partial_{yy}\tilde{u}$ should also be a constant. Applying the boundary conditions $\tilde{u}=0$ for $y=-H/2$ and $y=H/2$ yields:

$$\tilde{u} = \left[1 - \frac{4}{H^2}y^2\right]\tilde{u}_0.$$

However, if we again consider that at the inflow boundary $\tilde{u}=0$, and given that the adjoint velocity field is divergence-free, then in any section of x we must have:

$$\int \tilde{u} dy = 0,$$

which implies that the only possible solution is $\tilde{u}(x,y)=0$, and therefore:

$$-\partial_x \tilde{p} = \frac{\rho}{\mu}\partial_x p.$$

As at the exit the pressure p vanishes, i.e. $p=0$, we finally obtain the remarkable result that:

$$-\tilde{p} = \frac{\rho}{\mu} p,$$

i.e. the pressure and adjoint pressure are related by the factor $\frac{\rho}{\mu}$ and have a constant gradient in the field.

A.3. Exact derivatives of cost functions

Kinetic Energy:

$$I^{ke} = \frac{1}{2}\int \rho |\boldsymbol{u}|^2 \, \mathrm{dx}.$$

Given that $u = u(y), v = 0$ this results in:

$$I^{ke} = \frac{1}{2}\rho \int_x dx \int_y u^2 dy = \frac{1}{2}\rho L \int u_0^2 \left[1 - \frac{4}{H^2} y^2\right]^2 dy$$

$$I^{ke} = \frac{1}{2}\frac{8}{15} L H \rho u_0^2 \ ,$$

$$I^{ke}_{,u_0} = \frac{8}{15} L H \rho u_0 = \frac{2}{3} H \tilde{p}_{in} \ ,$$

i.e. linear in the length L and the velocity u_0, and

$$I^{ke}_{,x} = \frac{1}{2}\frac{8}{15} H \rho u_0^2 = \frac{1}{2}\frac{2}{3} H \tilde{p}_{in} u_0 \ ,$$

i.e. not dependent (constant) of the length L and quadratic in the velocity u_0. In the previous equations we assumed $p_{out} = 0$, and used the analytical results that relate mass flow, viscosity and pressure gradient for the Poiseuille flow. One should remark that if the domain that is of interest does not change (e.g. only a certain region inside the channel is considered), the correct value is:

$$I^{ke}_{,x} = 0$$

as the flow is constant in x and therefore the cost functional does not change if the upstream boundary is moved.

Vortical Energy (Dissipation):

$$I^{ve} = \frac{1}{2}\int \rho |\nabla \times \boldsymbol{u}|^2 \, \mathrm{dx}.$$

Given that $u = u(y), v = 0$ this results in:

$$I^{ve} = \frac{1}{2}\rho \int_x dx \int_y |\partial_y u|^2 dy = \frac{8}{3}\frac{\rho u_0^2}{H^2} L H$$

This implies:

$$I^{ve}_{,u_0} = \frac{16}{3} L \rho \frac{u_0}{H} = \frac{2 L H \tilde{p}}{3} \ ,$$

i.e. linear in the length L and the velocity u_0, and

$$I^{ve}_{,x} = \frac{8}{3}\frac{\rho u_0^2}{H} = \frac{L H \tilde{p} u_0}{3} \ ,$$

i.e. not dependent (constant) of the length L and quadratic in the velocity u_0. Notice, though, that as before if the domain that is of interest does not change (e.g. only a certain region inside the channel is considered), the correct value is:

$$I^{ve}_{,x} = 0$$

as the flow is constant in x and the cost functional will not change if the upstream boundary is moved.

References

[1] N. Amigo, A. Valencia, W. Wu, S. Patnaik, E. Finol, Cerebral aneurysm rupture status classification using statistical and machine learning methods, Proc. Inst. Mech. Eng., H J. Eng. Med. 235 (2021) 655–662, https://doi.org/10.1177/09544119211000477.

[2] H. Antil, R. Glowinski, R.H.W. Hoppe, C. Linsenmann, T.W. Pan, A. Wixforth, Modeling, simulation, and optimization of surface acoustic wave driven microfluidic biochips, J. Comput. Math. 28 (2010) 149–169.

[3] H. Antil, D.P. Kouri, M.D. Lacasse, D. Ridzal (Eds.), Frontiers in PDE-Constrained Optimization, The IMA Volumes in Mathematics and Its Applications, vol. 163, Springer, New York, 2018, papers based on the workshop held at the Institute for Mathematics and its Applications, Minneapolis, MN, June 6–10, 2016.

[4] M.A. Castro, Computational Hemodynamics of Cerebral Aneurysms, George Mason University, 2006.

[5] J.R. Cebral, M.A. Castro, O. Soto, R. Löhner, N. Alperin, Blood-flow models of the circle of Willis from magnetic resonance data, J. Eng. Math. 47 (2003) 369–386.

[6] F.J. Detmer, B.J. Chung, C. Jimenez, F. Hamzei-Sichani, D. Kallmes, C. Putman, J.R. Cebral, Associations of hemodynamics, morphology, and patient characteristics with aneurysm rupture stratified by aneurysm location, Neuroradiology (2018), https://doi.org/10.1007/s00234-018-2135-9.

[7] F.J. Detmer, B.J. Chung, C. Jimenez, F. Hamzei-Sichani, D. Kallmes, C. Putman, J.R. Cebral, Associations of hemodynamics, morphology, and patient characteristics with aneurysm rupture stratified by aneurysm location, Neuroradiology 61 (2019) 275–284.

[8] F.J. Detmer, B.J. Chung, F. Mut, M. Pritz, M. Slawski, F. Hamzei-Sichani, D. Kallmes, C. Putman, C. Jimenez, J.R. Cebral, Development of a statistical model for discrimination of rupture status in posterior communicating artery aneurysms, Acta Neurochirurg. 160 (2018) 1643–1652, https://doi.org/10.1007/s00701-018-3595-8.

[9] F.J. Detmer, D. Lückehe, F. Mut, M. Slawski, S. Hirsch, Comparison of statistical learning approaches for cerebral aneurysm rupture assessment, Int. J. Comput. Assisted Radiol. Surg. 15 (2020) 141–150, https://doi.org/10.1007/s11548-019-02065-2.

[10] F.J. Detmer, F. Mut, M. Slawski, S. Hirsch, P. Bijlenga, J.R. Cebral, Incorporating variability of patient inflow conditions into statistical models for aneurysm rupture assessment, Acta Neurochirurg. 162 (2020) 553–566.

[11] F.J. Foss II, R. Glowinski, When Bingham meets Bratu: mathematical and computational investigations, ESAIM Control Optim. Calc. Var. 27 (2021) 27, https://doi.org/10.1051/cocv/2021020.

[12] R. Glowinski, J. He, On shape optimization and related issues, in: Computational Methods for Optimal Design and Control, Arlington, VA, 1997, in: Progr. Systems Control Theory, vol. 24, Birkhäuser Boston, Boston, MA, 1998, pp. 151–179.

[13] R. Glowinski, Y. Song, X. Yuan, H. Yue, Bilinear optimal control of an advection-reaction-diffusion system, SIAM Rev. 64 (2022) 392–421, https://doi.org/10.1137/21M1389778.

[14] M.D. Gunzburger, L.S. Hou, T.P. Svobodny, Optimal control and optimization of viscous, incompressible flows, in: Incompressible Computational Fluid Dynamics: Trends and Advances, Cambridge Univ. Press, Cambridge, 2008, pp. 109–150.

[15] S. Hadad, F. Mut, M. Slawski, A.M. Robertson, J.R. Cebral, Evaluation of predictive models of aneurysm focal growth and bleb development using machine learning techniques, J. Neurointervent. Surg. (2023), https://doi.org/10.1136/jnis-2023-020241.

[16] J.W. He, M. Chevalier, R. Glowinski, R. Metcalfe, A. Nordlander, J. Periaux, Drag reduction by active control for flow past cylinders, in: Computational Mathematics Driven by Industrial Problems, Martina Franca, 1999, in: Lecture Notes in Math., vol. 1739, Springer, Berlin, 2000, pp. 287–363.

[17] M. Hinze, R. Pinnau, M. Ulbrich, S. Ulbrich, Optimization with PDE Constraints, Mathematical Modelling: Theory and Applications, vol. 23, Springer, New York, 2009.

[18] K. Ito, K. Kunisch, Lagrange Multiplier Approach to Variational Problems and Applications, Advances in Design and Control, vol. 15, Society for Industrial and Applied Mathematics (SIAM), Philadelphia, PA, 2008.

[19] K. Ito, S.S. Ravindran, Optimal control of thermally convected fluid flows, SIAM J. Sci. Comput. 19 (1998) 1847–1869, https://doi.org/10.1137/S1064827596299731.

[20] A. Jameson, W. Schmidt, E. Turkel, Numerical solution of the Euler equations by finite volume methods using Runge Kutta time stepping schemes, in: 14th Fluid and Plasma Dynamics Conference, 1981, p. 1259.

[21] G. Janiga, L. Daróczy, P. Berg, D. Thévenin, M. Skalej, O. Beuing, An automatic CFD-based flow diverter optimization principle for patient-specific intracranial aneurysms, J. Biomech. 48 (2015) 3846–3852, https://doi.org/10.1016/j.jbiomech.2015.09.039.

[22] D.F. Kallmes, W. Brinjikji, S. Cekirge, D. Fiorella, R.A. Hanel, P. Jabbour, D. Lopes, P. Lylyk, C.G. McDougall, A. Siddiqui, Safety and efficacy of the Pipeline embolization device for treatment of intracranial aneurysms: a pooled analysis of 3 large studies, J. Neurosurg. 127 (2017) 775–780, https://doi.org/10.3171/2016.8.JNS16467.

[23] M. Kotowski, O. Naggara, T.E. Darsaut, S. Nolet, G. Gevry, E. Kouznetsov, J. Raymond, Safety and occlusion rates of surgical treatment of unruptured intracranial aneurysms: a systematic review and meta-analysis of the literature from 1990 to 2011, J. Neurol. Neurosurg. Psychiatry 84 (2013) 42–48, https://doi.org/10.1136/jnnp-2011-302068.

[24] I. Larrabide, A.J. Geers, H.G. Morales, P. Bijlenga, D.A. Rüfenacht, Change in aneurysmal flow pulsatility after flow diverter treatment, Comput. Med. Imaging Graph. 50 (2016) 2–8, https://doi.org/10.1016/j.compmedimag.2015.01.008.

[25] J.L. Lions, Optimal Control of Systems Governed by Partial Differential Equations, Die Grundlehren der Mathematischen Wissenschaften, vol. 170, Springer-Verlag, New York-Berlin, 1971. Translated from the French by S.K. Mitter.

[26] R. Löhner, Applied Computational Fluid Dynamics Techniques: An Introduction Based on Finite Element Methods, John Wiley & Sons, 2008.

[27] P. Lylyk, C. Miranda, R. Ceratto, A. Ferrario, E. Scrivano, H.R. Luna, A. Berez, Q. Tran, P.K. Nelson, D. Fiorella, Curative endovascular reconstruction of cerebral aneurysms with the pipeline embolization device: the Buenos Aires experience, Neurosurgery 64 (2009) 632–642.

[28] H. Meng, V.M. Tutino, J. Xiang, A. Siddiqui, High WSS or low WSS? Complex interactions of hemodynamics with intracranial aneurysm initiation, growth, and rupture: toward a unifying hypothesis, Am. J. Neuroradiol. 35 (2014) 1254–1262, https://doi.org/10.3174/ajnr.A3558.

[29] E. Mestreau, R. Löhner, S. Aita, Tgv tunnel entry simulations using a finite element code with automatic remeshing, in: 31st Aerospace Sciences Meeting, 1993, p. 890.

[30] Y. Murayama, S. Fujimura, T. Suzuki, H. Takao, Computational fluid dynamics as a risk assessment tool for aneurysm rupture, Neurosurgical Focus 47 (2019) E12, https://doi.org/10.3171/2019.4.FOCUS19189.

[31] F. Mut, R. Löhner, A. Chien, S. Tateshima, F. Viñuela, C. Putman, J.R. Cebral, Computational hemodynamics framework for the analysis of cerebral aneurysms, Int. J. Numer. Methods Biomed. Eng. 27 (2011) 822–839.

[32] O.N. Naggara, P.M. White, F. Guilbert, D. Roy, A. Weill, J. Raymond, Endovascular treatment of intracranial unruptured aneurysms: systematic review and meta-analysis of the literature on safety and efficacy, Radiology 256 (2010) 887–897, https://doi.org/10.1148/radiol.10091982.

[33] J. Peraire, J. Peiró, K. Morgan, A 3d finite element multigrid solver for the Euler equations, in: 30th Aerospace Sciences Meeting and Exhibit, 1992, p. 449.

[34] A.M. Ramos, R. Glowinski, J. Periaux, Nash equilibria for the multiobjective control of linear partial differential equations, J. Optim. Theory Appl. 112 (2002) 457–498, https://doi.org/10.1023/A:1017981514093.

[35] S.S. Ravindran, Numerical solutions of optimal control for thermally convective flows, Int. J. Numer. Methods Fluids 25 (1997) 205–223, https://doi.org/10.1002/(SICI)1097-0363(19970730)25:2<205::AID-FLD547>3.3.CO;2-E.

[36] N.K. de Rooij, F.H. Linn, J.A. van der Plas, A. Algra, G.J. Rinkel, Incidence of subarachnoid haemorrhage: a systematic review with emphasis on region, age, gender and time trends, J. Neurol. Neurosurg. Psychiatry 78 (2007) 1365–1372.

[37] D.M. Sforza, C.M. Putman, J.R. Cebral, Hemodynamics of cerebral aneurysms, Annu. Rev. Fluid Mech. 41 (2009) 91–107, https://doi.org/10.1146/annurev.fluid.40.111406.102126.

[38] M. Shojima, M. Oshima, K. Takagi, R. Torii, M. Hayakawa, K. Katada, A. Morita, T. Kirino, Magnitude and role of wall shear stress on cerebral aneurysm: computational fluid dynamic study of 20 middle cerebral artery aneurysms, Stroke 35 (2004) 2500–2505.

[39] M.A. Silva, S. Chen, R.M. Starke, Unruptured cerebral aneurysm risk stratification: background, current research, and future directions in aneurysm assessment, Surgical Neurology International 13 (2022) 182, https://doi.org/10.25259/SNI_1112_2021.

[40] S. Soldozy, P. Norat, M. Elsarrag, A. Chatrath, J.S. Costello, J.D. Sokolowski, P. Tvrdik, M.Y.S. Kalani, M.S. Park, The biophysical role of hemodynamics in the pathogenesis of cerebral aneurysm formation and rupture, Neurosurgical Focus 47 (2019) E11, https://doi.org/10.3171/2019.4.FOCUS19232.

[41] D.A. Steinman, Image-based CFD modeling in realistic arterial geometries, Ann. Biomed. Eng. 30 (2004) 483–497.

[42] S. Tanioka, F. Ishida, A. Yamamoto, S. Shimizu, H. Sakaida, M. Toyoda, N. Kashiwagi, H. Suzuki, Machine learning classification of cerebral aneurysm rupture status with morphologic variables and hemodynamic parameters. Radiology, Artif. Intell. 2 (2020) e190077, https://doi.org/10.1148/ryai.2019190077.

[43] F. Tröltzsch, Optimal control of partial differential equations, in: Theory, Methods and Applications, in: Graduate Studies in Mathematics, vol. 112, American Mathematical Society, Providence, RI, 2010. Translated from the 2005 German original by Jürgen Sprekels.

[44] S.W. Walker, M.J. Shelley, Shape optimization of peristaltic pumping, J. Comput. Phys. 229 (2010) 1260–1291, https://doi.org/10.1016/j.jcp.2009.10.030.
[45] J. Xiang, S.K. Natarajan, M. Tremmel, D. Ma, J. Mocco, L.N. Hopkins, A.H. Siddiqui, E.I. Levy, H. Meng, Hemodynamic-morphologic discriminants for intracranial aneurysm rupture, Stroke 42 (2011) 144–152.
[46] J. Zowe, S. Kurcyusz, Regularity and stability for the mathematical programming problem in Banach spaces, Appl. Math. Optim. 5 (1979) 49–62.